Kinetic Study of the Asymmetric Hydrogenation of Methyl Acetoacetate in the Presence of a Ruthenium Binaphthophosphepine Complex

Eva Öchsner,[a] Bastian Etzold,[a] Kathrin Junge,[b] Matthias Beller,[b,*] and Peter Wasserscheid[a,*]

[a] Lehrstuhl für Chemische Reaktionstechnik, Universität Erlangen-Nürnberg, Egerlandstr. 3, 91058 Erlangen, Germany
Fax: (+49)-9131-852-7421; e-mail: Peter.Wasserscheid@crt.cbi.uni-erlangen.de
[b] Leibniz-Institut für Katalyse e.V. an der Universität Rostock, Albert-Einstein-Str.29a, 18059 Rostock, Germany
Fax: (+49) 381-1281-5000; e-mail: Matthias.Beller@catalysis.de

Abstract: The asymmetric hydrogenation of methyl acetoacetate (MAA) in methanol using dibromobis{(S)-4-phenyl-4,5-dihydro-3H-dinaphtho[2,1-c:1′,2′-e]phosphepine}-ruthenium was studied in detail. For the determination of the reaction network, data from kinetic experiments were compared to different possible reaction networks using the kinetic software Presto Kinetics. The simulation was optimised to describe the reaction accurately with a minimal set of process parameters and reaction equations. For the best model the reaction orders, collision factors and activation energy of all reaction steps were determined. Additionally, the influence of reaction temperature and hydrogen pressure on the enantiomeric excess (ee) of the reaction was studied. It was found that high reaction temperatures and high hydrogen pressures result in increasing enantioselectivities.

Keywords: asymmetric catalysis; asymmetric hydrogenation; hydrogenation; keto esters; ketones; kinetic study

Introduction

Today, asymmetric hydrogenation plays an important role in the production of chiral compounds and intermediates. In particular, asymmetric hydrogenations are applied for the commercial manufacture of pharmaceuticals, for example, naproxen, vitamin E, β-lactam antibiotics and adrenaline.[1,2] Moreover, asymmetric hydrogenation processes are also used in the synthesis of perfumery ingredients, intermediates of fine chemicals and for the development of new materials like ferro-electric liquid crystals and biodegradable polymers.[1,3]

In the past the development of asymmetric hydrogenation was significantly based on the synthesis of novel catalysts and suitable chiral ligands.[4,5,6,7] A particularly successful type of chiral ligand is the axially dissymmetric bisphosphine ligand BINAP which has been developed in the early 1980s.[8] Using this new ruthenium/BINAP complexes a wide range of functionalised olefins ranging from α-arylacrylic acids through α,β- and β,γ-unsaturated carboxylic acid to allylic alcohols as well as ketones could be hydrogenated with high selectivity and yield. In 2000, several monodentate phosphorus ligands with a 2,2′-binaphthol core were introduced.[9,10,11] The easier preparation of these monodentate ligands proved to be an essential advantage compared to most known bidentate ligands.[12]

Surprisingly, for asymmetric hydrogenation reactions detailed kinetic and thermodynamic studies are rarely found in literature. However, for a deeper understanding of the respective reaction it is essential to describe its properties with kinetic and thermodynamic parameters, in particular if more than one reaction mechanism is principally possible. In such case a detailed kinetic analysis can help to identify the most appropriate mechanistic model as the latter describes the experimental results with the smallest set of independent parameters and in the most accurate way.

In this study kinetics models are used to deduce possible reaction pathways for the asymmetric hydrogenation of methyl acetoacetate (MAA). Therefore, a large number of hydrogenation experiments have

been carried out and kinetic models have been derived from the respective concentration/time curves at different temperatures and hydrogen pressures. We want to introduce this approach as a valuable and fast method for the discrimination of different reaction pathways. It is noteworthy, however, that our study builds uniquely on the analysis of reaction products detectable by GC from the reaction mixture. Therefore we cannot exclude that short-living intermediates play a role in the molecular mechanism of the reaction.

In this contribution, the kinetics of the hydrogenation of methyl acetoacetate (MAA) to *R/S*-methyl hydroxybutyrate (MHB) are described in detail. In our study dibromobis[(*S*)-4-phenyl-4,5-dihydro-3*H*-dinaphtho[2,1-*c*:1′,2′-*e*]phosphepine]ruthenium is used as the homogeneous catalyst (Figure 1). In 2005 this Ru complex was first published by some of us[12a] and the ligand has been used in various asymmetric hydrogenations.[12b–e]

In most catalytic asymmetric hydrogenations, alcohols and halogen-containing hydrocarbons like CH_2Cl_2 are applied as solvents. As an example, the asymmetric hydrogenation of MAA with phosphorus ligands has been reported to show the highest activity and enantioselectivity in alcoholic solvents, in particular in methanol.[13,14] Therefore, we used methanol as the solvent for our kinetic studies.

If the hydrogenation reaction of MAA is performed in methanol, ketal and hemiketal intermediates are formed. Obviously, these parallel reactions are reversible equilibrium reactions. Figure 2 shows the formal reaction scheme as it was known from the literature[15] when we started the detailed kinetic studies described in this publication.

Note that the reported formal reaction scheme shows the formation of ketal and hemiketal compounds, but no hydrogenation of these compounds.

Hence, a major aim of this study was to check the proposed reaction network of the hydrogenation reaction in methanol by comparison of the experimental kinetic results with several possible kinetic models. For the most suitable model, reaction orders, collision factors and the activation energy have been determined for all reaction steps.
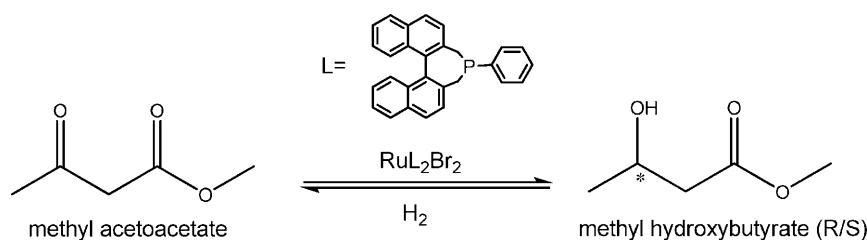
Figure 1. Hydrogenation of MAA using dibromobis[(*S*)-4-phenyl-4,5-dihydro-3*H*-dinaphtho[2,1-*c*:1′,2′-*e*]phosphepine]ruthenium as catalyst.
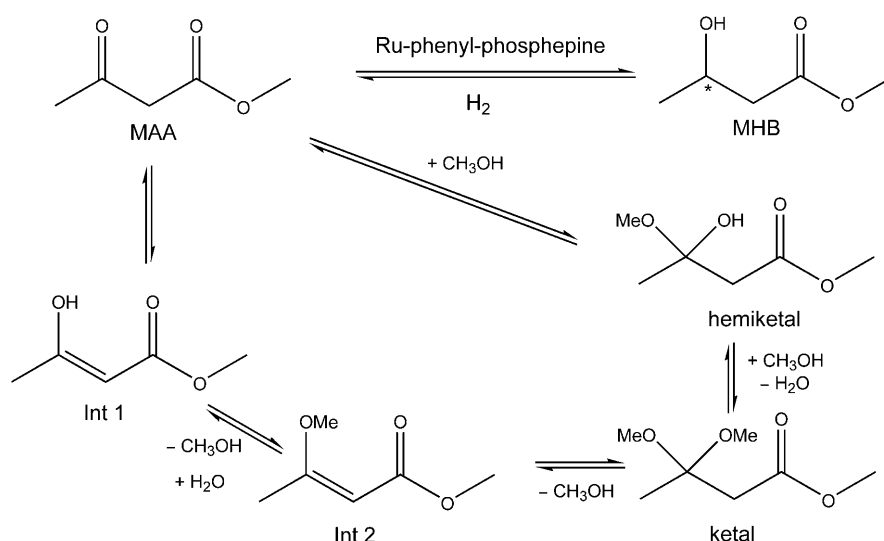
Figure 2. Formal reaction scheme of MAA hydrogenation similar to ref.[15]

Results and Discussion

Determination of the Reaction Network

Figure 3 shows the concentration profiles of all liquid reactants during a typical hydrogenation experiment (more experimental data including reproduction runs and hydrogenation runs at different temperatures and pressures can be found in the Supporting Information). The results of the kinetic modelling (discussed in detail in the section "Estimation of Kinetic Parameters" below) are indicated as dotted lines.

In the first 20 min of the experiment a fast decrease of MAA is observed which is obviously not due to MAA hydrogenation but is caused by the rapid formation of the ketal and hemiketal intermediates. During the course of the reaction, the concentrations of ketal and hemiketal intermediates run through a maxima ($t_{max,ketal} = 20$ min, $t_{max,hemiketal} = 100$ min) while the formation of the MHB product increases in an almost linear fashion over reaction time.

Apparently, these results agree in principle with the formal reaction scheme in Figure 2. However, we were interested to check whether this reported reaction scheme would indeed give the best description of the observed concentration *vs.* time curves or whether alternative models of the reaction network would allow for a better agreement with the experimental kinetic data. Therefore alternative reaction networks have been tested in the kinetic modelling with the aim to identify the model that describes with the lowest number of parameters the experimental results in the most accurate manner.

All modelling work has been carried out using the software Presto Kinetics (CiT GmbH, Germany, version 7.2.1). To obtain the differential equations for modelling, equations for formation and consumption of all reactants [Eq. (1)] and power law rate expressions [Eq. (2)] for all reaction steps were assumed (for details see section "Estimation of Kinetic Parameters" below).

$$R_i = \sum_{j=1}^{M} \upsilon_{ij} \cdot r_j \tag{1}$$

$$r = k \cdot \prod_i c_i^{mi} \tag{2}$$

For solving the differential equations, the following simplifications and assumption were made. All experiments were carried out with the same catalyst concentration. Therefore the catalyst concentration was not accounted for in the modelling. The concentration of the solvent methanol was in excess to the substrate MAA and remained quasi constant during reaction. The concentration of water during the reaction is unknown. Only water-free solvent and reactants were utilised, but water produced during the reaction could not be analysed. Thus, no water-dependent reaction rates were derived. The hydrogen solubility was assumed to change only marginally during the experiments. Consequently, the hydrogen partial pressure was utilised directly in the reaction rate equations instead of the hydrogen concentration.

Ketal and hemiketal formation are strongly influenced by thermodynamics. Therefore, the equilibrium constants need to be known for an accurate description of the kinetics. With these constants [determined according to Eq. (3)] the reaction rate constant of the
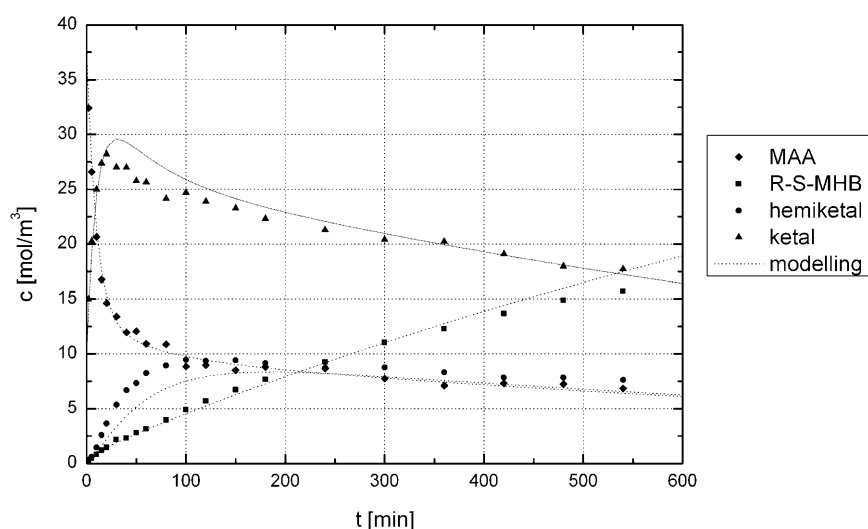
Figure 3. Concentration profiles of all liquid reactants during the MAA hydrogenation in methanol. *Reaction conditions: T =* 80 °C, $p(H_2) = 10$ bar, stirrer speed = 1200 rpm, S/C = 259.

$$K_i = \exp\left(\frac{-\Delta_R H_i^0}{R \cdot T} + \frac{-\Delta_R S_i^0}{R}\right) \qquad (3)$$

reversible reactions was calculated [see Eqs. (10)–(15) in section "Estimation of Kinetic Parameters" below].

In the studied temperature region (60–120 °C), the standard reaction enthalpy ($\Delta_R H_{i\,MAA-K}^0 = -22.96$ kJ mol^{-1}, $\Delta_R H_{i\,K-HK}^0 = 42.75$ kJ mol^{-1}, $\Delta_R H_{i\,MAA-HK}^0 = -40.01$ kJ mol^{-1}) and entropy ($\Delta_R S_{i\,MAA-K}^0 = -57.05$ J mol^{-1} K^{-1}, $\Delta_R S_{i\,K-HK}^0 = 113$ J mol^{-1} K^{-1}, $\Delta_R S_{i\,MAA-HK}^0 = 114.4$ J mol^{-1} K^{-1}) are assumed to be constant. The values have been derived by fitting Eq. (3) to the measured equilibrium constants. The measured equilibrium constants were determined from concentration *vs.* reaction time plots. It is assumed that equilibrium is reached when the ratios over the reaction time converge to a final value. This procedure is possible as the reversible reactions are faster than the hydrogenation reactions.

Table 1 shows the calculated equilibrium constants for the reaction of MAA to hemiketal, from MAA to ketal and from ketal to hemiketal intermediate.

At this point, all basic equations and settings for the modelling are defined and the modelling results for the different reaction network can be compared to the experimental data. For this comparison, the residual (given from the parameter estimation done by the

minimisation of the least squares objective function of absolute values by the damped Gauss–Newton algorithm) is determined for all tested models. The model with the lowest residual fits best if the number of independent parameters in all different models is comparable.

As a first benchmark, the proposed reaction scheme[15] was adapted for its utilisation as a kinetic reaction network. In this adaption, all reaction steps including experimentally non-detectable intermediates (namely Int 1 and Int 2 from Figure 2) were omitted. Consequently, only the hydrogenation of MAA and the parallel equilibrium reactions of MAA to K, K to HK and MAA to HK are considered in model 1 (Figure 4 left).

The residual (representing the degree of fit between the simulated and the measured data) was found to be 0.296 for model 1. As a first variation of this model, we tested the elimination of the reversible reaction between MAA and HK in model 2. Interestingly, this variation did not result in a significant change of the model fit, the same residual of 0.296 was obtained. Consequently, to fulfil the aim of a kinetic description with a minimum of parameters in a more formalistic manner, this reaction step should be omitted from the kinetic model. However, a reasonable molecular mechanistic view on the reaction would always require to consider the MAA–HK equilibrium reaction step as the direct formation of ketal is difficult to imagine without a hemiketal intermediate. For this reason and in the light of the identical fit of the two models, we decided to include the MAA–HK equilibrium in all further models.

A more detailed comparison of the experimental and simulated results for models 1 and 2 revealed that the equilibrium reactions are described accurately, but the concentration of the product MHB is simulated systematically wrong for high pressures and temperatures. This led us to the assumption that the hydrogenation reaction to MHB differs from models 1 and 2. Hence, also models that do not include a direct hydrogenation of MAA have been tested
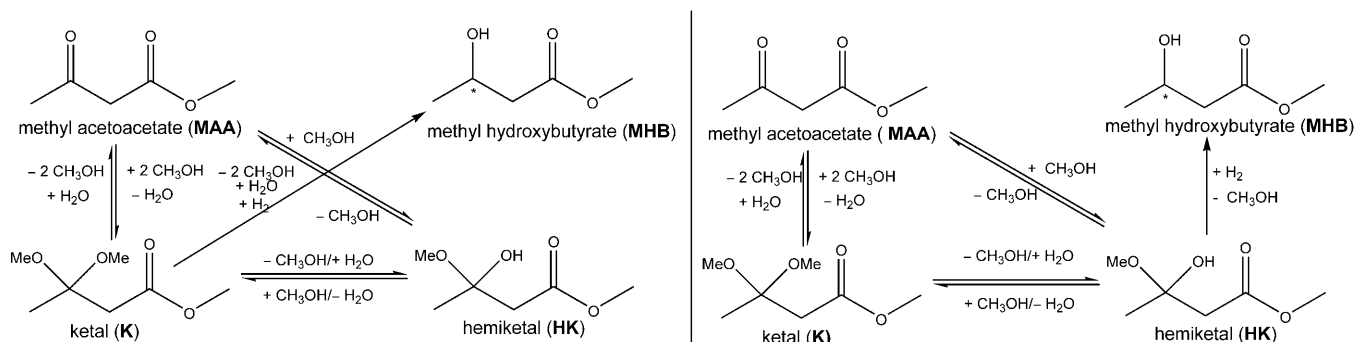
Table 1. Calculated equilibrium constants for the ketal/hemiketal formation of MAA in methanol.[a]

T [°C]	K_{MAA-K}	K_{K-HK}	K_{MAA-HK}
60	4.2	0.2	2.0
80	2.6	0.4	0.9
90	2.1	0.6	0.6
100	1.7	0.8	0.4
120	1.2	1.7	0.2

[a] Reaction conditions: $T = 60$–120 °C, $p(H_2) = 5$–20 bar, stirrer speed = 1200 rpm, S/C = 259.
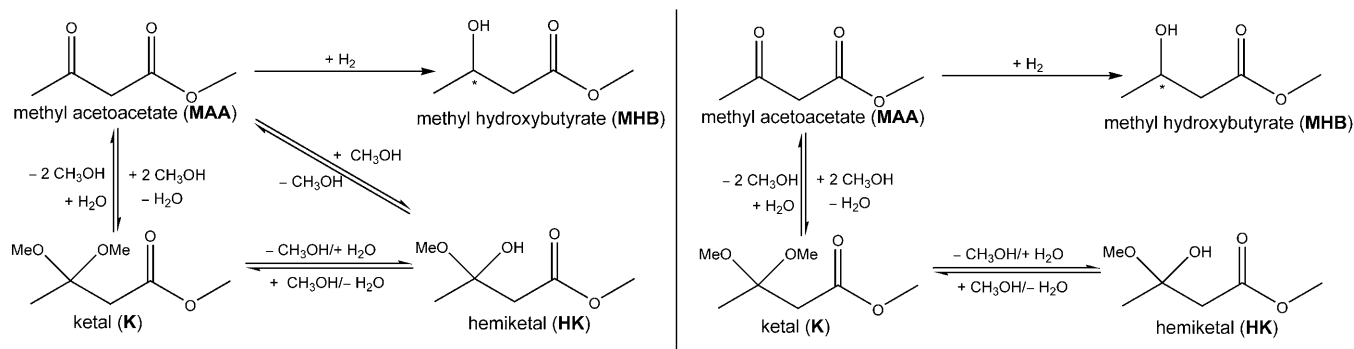
Figure 4. Reaction network models for the hydrogenation of MAA: model 1 (*left*) and model 2 (*right*).

Figure 5. Reaction networks for the hydrogenation of MAA: model 3 (*left*) and model 4 (*right*).

(Figure 5). Hydrogenation of the ketal intermediate (model 3) and hydrogenation of the hemiketal intermediate (model 4) were assumed to be the only MHB-forming steps, respectively.

Both models show high deviation from experimental data as the residual of model 3 was determined to 0.332 and the residual of model 4 to 0.484. These results correspond to literature reports, in which the asymmetric hydrogenation of MAA with similar ligands has also been described in a non-alcoholic solvent, such as dichloromethane.[13]

The simulations using models 3 and 4 revealed that the experimental concentration profiles can in principle also be fitted by hydrogenation reactions from the ketal or hemiketal intermediates to MHB, but in these cases the results of the temperature and hydrogen pressure variation is not represented well. This indicates that these reactions should not be ignored completely, and should be taken into consideration besides the direct hydrogenation of MAA.

Consequently, this led to models 5 and 6 (Figure 6) both containing the direct hydrogenation from MAA to MHB. Model 5 includes additionally the hydrogenation reaction from the ketal intermediate to MHB while model 6 accounts for the additional hydrogenation of the hemiketal intermediate to MHB.

Both networks showed – compared to models 1 to 4 – a clearly improved fit to the experimental kinetic

data. The residual of model 5 was determined as 0.257, the calculations based on model 6 resulted in a residual of 0.215. To illustrate the difference in the fit quality between the formal reaction network similar to the literature[15] (model 1) and the expanded models tested in this work, Figure 7 shows the parity plots of the MHB formation for models 1 and 6 in comparison. All parity plots based on model 6 show the best agreement of experimental and modelled data for the reactants. It is noteworthy that the additional consideration of a hydrogenation of the ketal intermediate in model 6 offered no improvement.

As a result of our kinetic studies and the comparison of the experimental data with different kinetic models we conclude that the literature proposed reaction network for the hydrogenation of MAA in methanol with Ru-BINAP complexes[15] differs from our Ru-phenylphosphepine-catalysed reaction network. The here proposed reaction network of model 6 shows a much better fit to the experimental data and explains easily the experimental fact that the asymmetric hydrogenation of MAA is significantly accelerated in alcoholic solvents. The additional hydrogenation step of hemiketal intermediate – which is only formed in alcoholic solvents – opens an additional pathway to the MHB formation and is necessary for the accurate kinetic description.
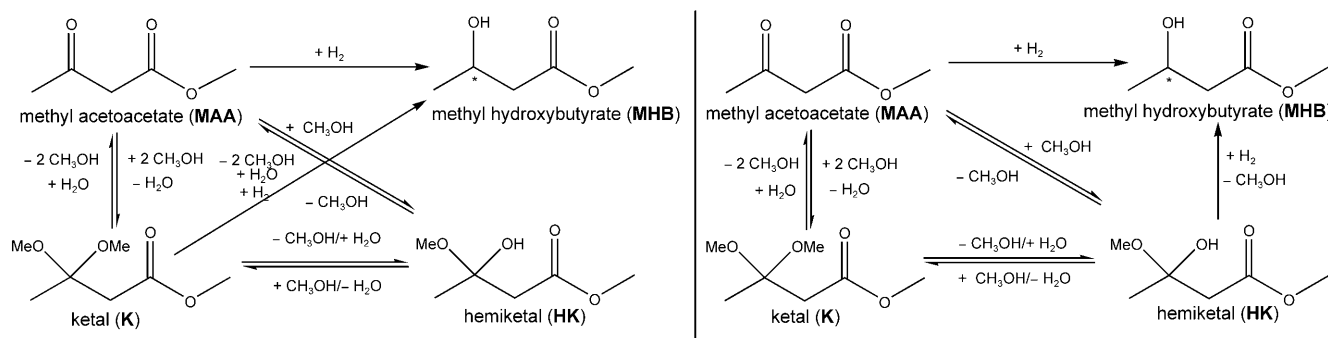
Figure 6. Reaction networks for the hydrogenation of MAA: model 5 (*left*) and model 6 (*right*).
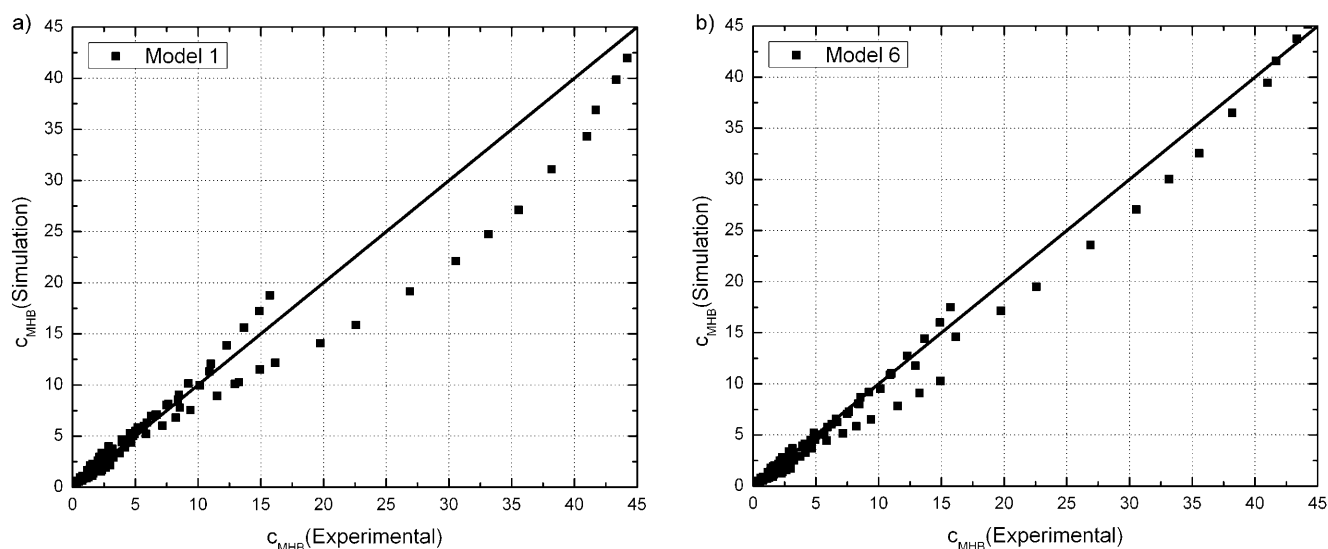
Figure 7. Parity plots for MHB (exemplary) based on model 1 and 6. *Reaction conditions:* $T = 60–120\,°C$, $p(H_2) = 5–20$ bar, stirrer speed = 1200 rpm, S/C = 259.

Estimation of Kinetic Parameters

For all six models kinetic parameters were fitted to calculate the residual of all models. In this section only the parameters for the most appropriate reaction model 6 are discussed. Figure 8 shows the simplified reaction network that has been generated from model 6.
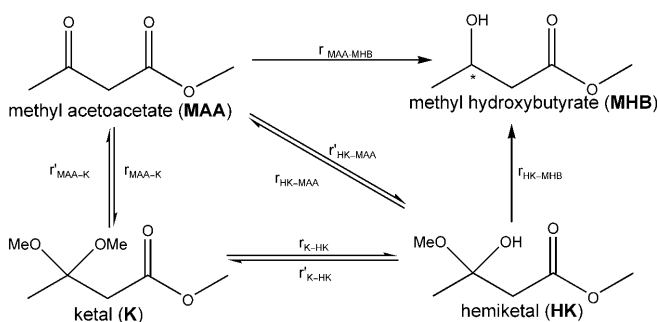
For the kinetic modelling, the following equations for the formation and consumption of all liquid reactants were applied.

$$R_{MAA} = r'_{MAA-K} - r_{MAA-K} - r_{MAA-MHB} - r'_{HK-MAA} + r_{HK-MAA} \quad (4)$$

$$R_{MHB} = r_{MAA-MHB} + r_{HK-MHB} \quad (5)$$

$$R_K = r_{MAA-K} - r'_{MAA-K} + r'_{K-HK} - r_{K-HK} \quad (6)$$

$$R_{HK} = r_{K-HK} - r'_{K-HK} - r_{HK-MHB} - r_{HK-MAA} + r'_{HK-MAA} \quad (7)$$

The individual reaction rates for the hydrogenation steps are given by Eqs. (8) and (9). The reaction rates for the equilibrium reaction are defined according to Eqs. (10)-(15).

To determine the reaction order of MAA, ketal intermediate K and hemiketal intermediate HK, experiments with constant hydrogen pressure have been carried out. This guaranteed the reaction rate to be unaffected by the availability of hydrogen in this set of experiments. The orders of all organic reactants were determined by the integral method, which involves fitting of the resulting concentration *vs.* time plots. As a result, the reaction orders of all organic liquid reactants (MAA, K and HK) were found to be 1. Similar data have been obtained in the literature for the

Figure 8. Reaction network developed from model 6 for the MAA hydrogenation in methanol.

$$r_{MAA-MHB} = k_{MAA-MHB} \cdot c_{MAA} \cdot p_{H2} \quad \text{with} \quad k_{MAA-MHB} = k_{0,MAA-MHB} \cdot e^{-\frac{E_{A,MAA-MHB}}{R \cdot T}} \quad (8)$$

$$r_{HK-MHB} = k_{HK-MBH} \cdot c_{HK} \cdot p_{H2} \quad \text{with} \quad k_{HK-MHB} = k_{0,HK-MHB} \cdot e^{-\frac{E_{A,HK-MHB}}{R \cdot T}} \quad (9)$$

$$r_{MAA-K} = k_{MAA-K} \cdot c_{MAA} \qquad \text{with} \qquad k_{MAA-K} = k_{0,MAA-K} \cdot e^{-\frac{E_{A,MAA-K}}{R \cdot T}} \qquad (10)$$

$$r'_{MAA-K} = k'_{MAA-K} \cdot c_K \qquad \text{with} \qquad k'_{MAA-K} = \frac{k_{MAA-K}}{K_{MAA-K}} \qquad (11)$$

$$r_{K-HK} = k_{K-MBH} \cdot c_K \qquad \text{with} \qquad k_{K-HK} = k_{0,K-HK} \cdot e^{-\frac{E_{A,K-HK}}{R \cdot T}} \qquad (12)$$

$$r'_{K-HK} = k'_{K-HK} \cdot c_{HK} \qquad \text{with} \qquad k'_{K-HK} = \frac{k_{K-HK}}{K_{K-HK}} \qquad (13)$$

$$r_{HK-MAA} = k_{HK-MAA} \cdot c_{HK} \qquad \text{with} \qquad k_{HK-MAA} = k_{0,HK-MAA} \cdot e^{-\frac{E_{A,HK-MAA}}{R \cdot T}} \qquad (14)$$

$$r'_{HK-MAA} = k'_{HK-MAA} \cdot c_{MAA} \qquad \text{with} \qquad k'_{HK-MAA} = \frac{k_{HK-MAA}}{K_{HK-MAA}} \qquad (15)$$

asymmetric hydrogenation of unsaturated carboxylic acids with Ru-BINAP systems (reaction order = 1)[16] and for the asymmetric hydrogenation of tiglic acid with Ru-BINAP systems (reaction order = 0.881–0.929).[17]

In another set of experiments the reaction order with respect to hydrogen was derived experimentally by varying the hydrogen pressure from 5 to 20 bar. The variation results in a linear relation between the rate coefficients and hydrogen pressure (Figure 9). Thus a first order with respect to hydrogen pressure was determined for all hydrogenation reactions. These results are in agreement with the work of Ashby et al.[16] and Dong et al.[17] They described Ru-catalysed hydrogenation reactions to be of first order in hydrogen at low hydrogen pressures because the het-

erolytic split of hydrogen by the ruthenium-olefin complex is the rate-determining step (rds). At higher hydrogen pressure, however, the reaction of the ruthenium complex with olefin becomes rate-determining and the reaction is zero order in hydrogen.[17]

The activation energies and collision factors have been determined from the experiments at different temperatures in the range between 60 °C and 120 °C. In Arrhenius plots, which are shown in Figure 10 and Figure 11, reaction coefficients were plotted against different reaction temperatures for all reaction pathways. The activation energy of the reaction has been calculated from the slope of the Arrhenius plot and the collision factor has been determined from the intersection with the y-axis. The resulting values are summarised with all kinetic parameters in Table 2.
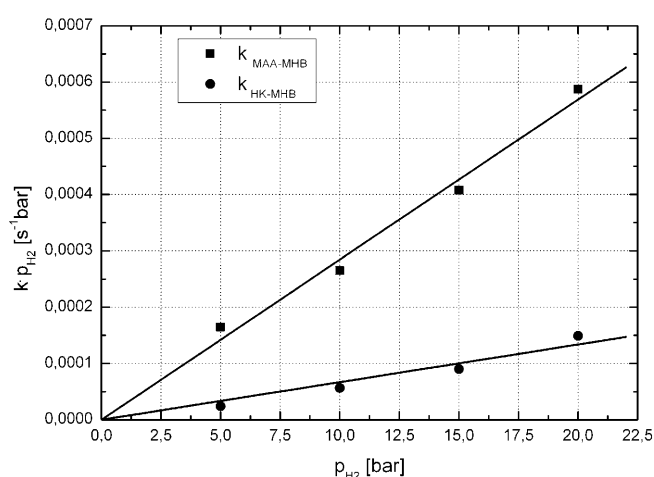
Figure 9. Reaction rates of hydrogenation steps (MAA–MHB and HK–MHB) as a function of different hydrogen pressures. *Reaction conditions: T = 80 °C, p(H₂) = 5–20 bar, stirrer speed = 1200 rpm, S/C = 259.*
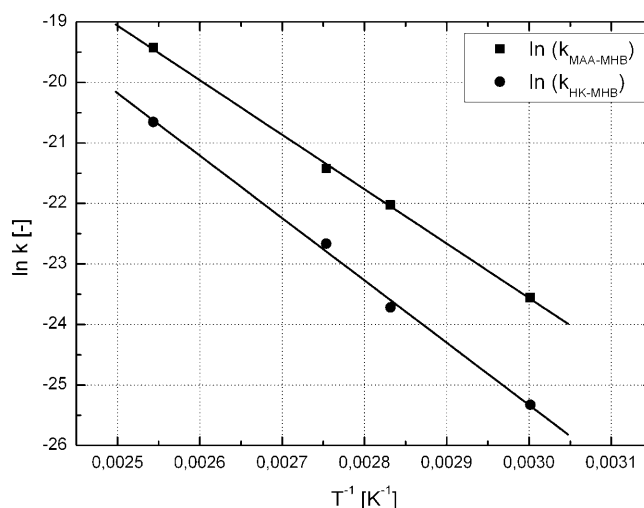
Figure 10. Arrhenius plots for different hydrogenation steps in the hydrogenation of MAA. *Reaction conditions: T = 60–120 °C, p(H₂) = 5–20 bar, stirrer speed = 1200 rpm, S/C = 259.*
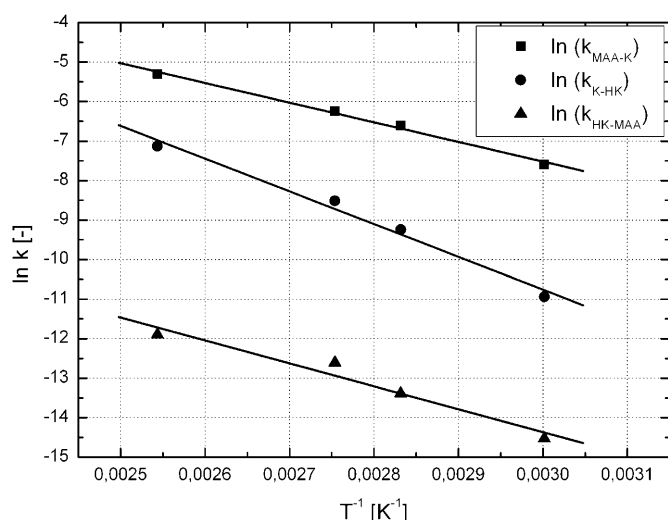
Figure 11. Arrhenius plot of the ketal and hemiketal formation reaction in the hydrogenation of MAA in methanol. *Reaction conditions:* $T = 60–120\,°C$, $p(H_2) = 5–20$ bar, stirrer speed $= 1200$ rpm, $S/C = 259$.

The activation energies for the hydrogenation reactions are in a range of 74.8–85.6 kJ·mol^{-1}. This range corresponds quite well to published literature data for other hydrogenation reactions with Ru complexes. For example, the group of Dong studied the asymmetric hydrogenation of tiglic acid catalysed by Ru-BINAP and Ru-(p-OCF$_3$)-BINAP systems and determined activation energies between 80.1–82.7 kJ·mol^{-1}.[17] Mahfud et al. calculated the activation energy of the hydrogenation of 1-hydroxy-2-propanone with RuCl$_2$(PPh$_3$)$_3$ to be 81 ± 17 kJ·mol^{-1}.[18] The activation energies of the ketal and hemiketal formation reactions were found to show lower values (41.4–68.8 kJ·mol^{-1}) compared to the hydrogenation reactions.

We also determined the reaction enthalpy for the total reaction from MAA to MHB. For this purpose the combustion enthalpies of MAA and MHB were measured in a calorimeter. The formation enthalpies of MAA (-657.7 kJ·mol^{-1}) and MHB (-721.3 kJ·mol^{-1}) were determined out of the combustion enthalpies. The formation enthalpy of hydrogen (-0.379 kJ·mol^{-1}) was found in literature.[19] The reaction enthalpy was calculated from the enthalpies of formation of every single reactant.

$$\Delta H_{R,T}^0 = \sum_i \nu_i \cdot (\Delta H_{f,T}^0)_i$$

The reaction enthalpy was determined to -63.2 kJ·mol^{-1} indicating a moderately exothermic reaction.

Influence of Reaction Temperature and Pressure on the Enantiomeric Excess

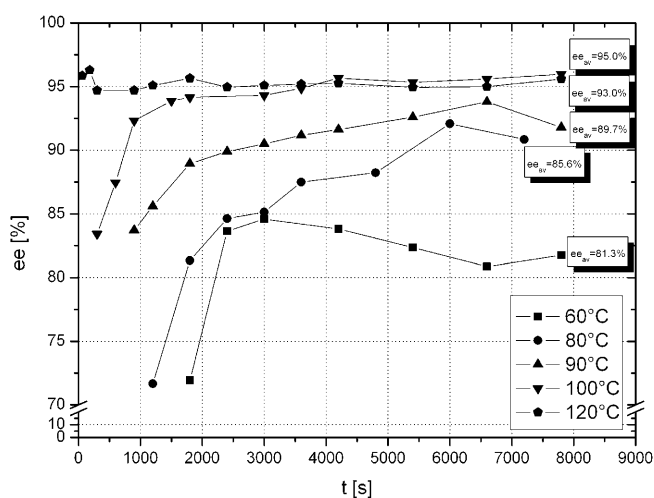The effect of the reaction temperature on the enantioselectivity was investigated in the range of 60°C–120°C. Figure 12 shows the *ee* profile and the average *ee* (ee_{av}) over the studied temperature range.

Remarkably, the *ee* is strongly dependent on the reaction temperature with higher temperatures leading to significantly higher enantiomeric excess (average *ee* of 81.3% at 60°C *vs.* 95.0% at 120°C). Within the reaction time the *ee* increases at the beginning of the reaction in the temperature range between 60°C and 100°C and remains constant after some kind of "activation period". This is different at 120°C where the *ee* shows an almost constant value over the whole reaction time. A possible explanation for the increasing *ee* in the early stages of the reaction at lower reaction temperature is the slow formation of the most selective catalyst species. In the literature[12] the unsteady *ee* of Ru complexes of binaphthophosphepine ligands is explained by the fact that the most selective catalyst species only forms after addition of the substrate. From our results we conclude that this formation process occurs much faster at 120°C and therefore an

Table 2. Collision factors and activation energies for the hydrogenation of MAA in methanol assuming a power law model.

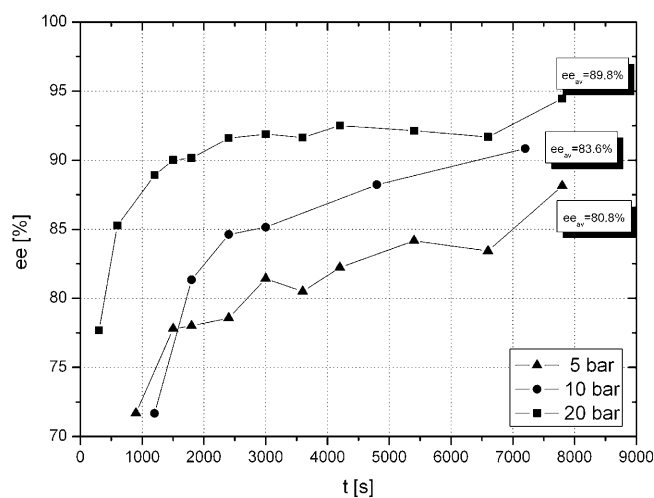| Variable	Value	[Unit]
$k_{0,\ MAA-MHB}$	6.01×10^0	Pa^{-1}·s^{-1}
$k_{0,\ HK-MHB}$	5.15×10^1	Pa^{-1}·s^{-1}
$k_{0,\ MAA-K}$	3.28×10^2	s^{-1}
$k_{0,\ K-HK}$	2.61×10^5	s^{-1}
$k_{0,\ HK-MAA}$	2.13×10^1	s^{-1}
$E_{A,\ MAA-MHB}$	74.8	kJ·mol^{-1}
$E_{A,\ HK-MHB}$	85.6	kJ·mol^{-1}
$E_{A,\ MAA-K}$	41.4	kJ·mol^{-1}
$E_{A,\ K-HK}$	68.8	kJ·mol^{-1}
$E_{A,\ HK-MAA}$	48.3	kJ·mol^{-1}

Figure 12. Effect of reaction temperature on enantioselectivity for the MAA hydrogenation in methanol. *Reaction conditions:* $T = 60$–$120\,°C$, $p(H_2) = 10$ bar, stirrer speed = 1200 rpm, S/C = 259.

Figure 13. Effect of hydrogen pressure on the enantioselectivity of the hydrogenation of MAA in methanol. *Reaction conditions:* $T = 80\,°C$, $p(H_2) = 5$–20 bar, stirrer speed = 1200 rpm, S/C = 259.

almost constant value of 95% *ee* is observed over the whole reaction time.

An additional explanation for the improved *ee* at high temperatures may arise from the mechanistic considerations discussed earlier in this paper. As it can be seen from Table 1, a high reaction temperature shifts significantly the equilibrium from MAA to ketal and hemiketal intermediates. This results in a higher concentration of ketal and hemiketal intermediates and favours the hydrogenation of the hemiketal intermediate. Also the higher activation energy of the hemiketal hydrogenation (85.6 kJ·mol^{-1}) compared to the hydrogenation of MAA (74.8 kJ·mol^{-1}) prefers the hemiketal hydrogenation at high reaction temperatures. As higher temperature favours the formation of hemiketal and leads to significantly higher *ee* we conclude that the hydrogenation of the hemiketal leads to a higher enantioselectivity compared to the direct hydrogenation of MAA.

Finally, the influence of hydrogen pressure on the enantioselectivity was examined in the pressure range from 5 to 20 bar (Figure 13). Interestingly, an increasing hydrogen pressure resulted in clearly higher enantioselectivities. At 80°C, higher hydrogen pressures also led to a faster increase of *ee* in the course of the reaction. While at 20 bar hydrogen pressure an almost constant *ee* of 92% was reached after 2400 s reaction time, the *ee* was increasing steadily over 8000 s reaction time for the experiments at 5 bar and 10 bar reaching a maximum *ee* of 88.1% (5 bar H$_2$) and 90.9% (10 bar H$_2$), respectively.

Again, these results are in good agreement with literature reports of other Ru-catalysed asymmetric hydrogenation reactions. Combes et al.[20] reported for the Ru/BINAP-catalysed hydrogenation of 2-(6-me-

thoxy-2-naphthyl)propenoic acid in methanol decreasing enantioselectivities with lower pressure in the pressure range below 30 bar.

Conclusions

In summary, detailed kinetic studies of the asymmetric hydrogenation of methyl acetoacetate (MAA) using a dibromobis[(*S*)-4-phenyl-4,5-dihydro-3*H*-dinaphtho[2,1-*c*:1′,2′-*e*]phosphepine]ruthenium catalyst in methanol have been reported. The reaction proceeds *via* a reaction network consisting of hydrogenation steps and the reversible formation of hemiketal and ketal intermediates. Six possible reaction network models have been designed and tested for their suitability to describe this asymmetric hydrogenation in the most accurate way using the lowest number of independent parameters. By comparing the experimental kinetic data with fitted model data – determined by the kinetic software Presto – the best modelling results were obtained for model 6 (residual = 0.215) which includes hydrogenation steps from methyl acetoacetate (MAA) to methyl hydroxybutyrate (MHB) and from the hemiketal intermediate to MHB. For this network all kinetic parameters were determined. Reaction orders of all organic reactant and hydrogen were found to be 1. The activation energy of the hydrogenation reaction from MAA to MHB is in the range of 74.8–85.6 kJ·mol^{-1}.

Additionally, the influence of temperature and hydrogen pressure on the enantioselectivity was investigated. It was shown that reaction conditions favouring the hydrogenation of the hemiketal intermediate (i.e., high temperature influencing both the hemiketal

equilibrium and the hemiketal hydrogenation kinetics) led to significantly higher enantioselectivities. Moreover, a higher reaction temperature resulted in faster formation of the most selective catalyst species with almost constant *ee* of 95% over the whole reaction time for a reaction temperature of 120°C. A beneficial effect of higher hydrogen partial pressures was revealed in the pressure range of 5 to 20 bar.

Experimental Section

Chemicals

All chemicals applied in this study were commercially available and were used without further purification steps. MAA (99%) was purchased from Aldrich, hydrobromic acid (48%) from Fluka. Commercial dry methanol and acetone from Acros (both 99.9%, water content less than 50 ppm), bis(2-methoxyethyl) ether from Acros (99%, used as internal GC-standard) and [bis(2-methylallyl)(1,5-cyclooctadiene)ruthenium(II)] from Acros were used. (*S*)-4-Phenyl-4,5-dihydro-3*H*-dinaphtho[2,1-*c*:1′,2′-*e*]phosphepine was synthesised according to the literature.[12]

Catalyst Preparation

The catalyst was prepared in close analogy to former reports.[12] A mixture of one equivalent of [bis(2-methylallyl)(1,5-cyclooctadiene)ruthenium(II)] and two equivalents of (*S*)-4-phenyl-4,5-dihydro-3*H*-dinaphtho[2,1-*c*:1′,2′-*e*]phosphepine was placed in a Schlenk flask under argon atmosphere. Dry acetone (5 mL) and a solution (0.29 molar) of hydrobromic acid (0.33 mL) in methanol were added and the solution was stirred 30 min at room temperature. This solution was heated to 30°C in an oil bath and the solvent was removed under high vacuum for 1 h. After this procedure, the catalyst was obtained as a brown solid powder.

Catalytic Hydrogenation

All hydrogenation experiments were carried out in a 300-mL Parr stainless steel autoclave (type 316, see Figure 14) with gas entrainment stirrer and glass liner. The reactor was equipped with an internal cooling coil (cooling agent: water), a thermocouple (Ni-Cr-Ni), a pressure transducer, a purge gas valve, a sampling valve, a relief pressure valve, a gas inlet and a gas outlet.

Prior to every hydrogenation experiment, the catalyst was dissolved in 160 mL methanol and the resulting solution was stirred for one hour. Afterwards, the catalyst solution was transferred into the reactor under an argon atmosphere and MAA and the internal GC-standard bis(2-methoxyethyl) ether were added. Then the reactor was closed and purged with argon to remove the air. The autoclave was heated to the desired reaction temperature and charged with hydrogen. The reaction was initiated by starting the gas entrainment stirrer (1200 rpm). Samples were taken periodically through a sampling tube. The sampling line was completely flushed before every sampling to avoid falsification of results. All experiments were semi-batch as the hydrogen pressure was kept constant during reaction. The collected sam-
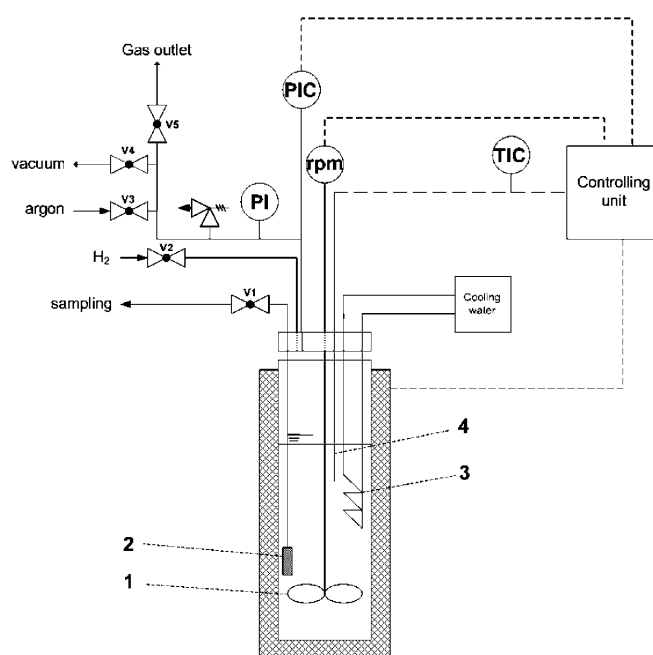
Figure 14. Experimetal set-up as used in the catalytic hydrogenation experiments: (1) gas entrainment stirrer, (2) sample line with frit, (3) cooling coil with cooling water, (4) thermocouple.

ples were filtered with syringe filters and were analysed by gas chromatography (Varian 3900 equipped with a Lipodex E column).

For the kinetic experiments, reaction temperatures (60–120°C) and hydrogen pressures (5–20 bar) were varied at a constant catalyst concentration (S/C = 259).

To determine the heat of formation (ΔH_R) of MAA and the hydrogenation product methyl hydroxybutyrate (MHB) the IKA-calorimeter "C400 adiabatic" was applied.

References

[1] S. Akutagawa, *Appl. Catal. A: General* **1995**, *128*, 171–207.

[2] F. D. Klingler, *Acc. Chem. Res.* **2007**, *40*, 1367–1376.

[3] L. A. Saudan, *Acc. Chem. Res.* **2007**, *40*, 1309–1319.

[4] W. S. Knowles, M. J. Sabacky, *J. Chem. Soc. (D)* **1968**, 1445–1446.

[5] W. S. Knowles, M. J. Sabacky, B. D. Vineyard, *J. Chem. Soc., Chem. Commun.* **1972**, 10.

[6] W. S. Knowles, *Angew. Chem.* **2002**, *114*, 2096–2107; *Angew. Chem. Int. Ed.* **2002**, *41*, 1998–2007.

[7] W. S. Knowles, R. Noyori, *Acc. Chem. Res.* **2007**, *40*, 1238–1239.

[8] R. Noyori, *Angew. Chem.* **2002**, *114*, 2108–2123; *Angew. Chem. Int. Ed.* **2002**, *41*, 2008–2022.

[9] M. T. Reetz, T. Sell, *Tetrahedron Lett.* **2000**, *41*, 6333–6336.

[10] L. A. Arnold, R. Imbos, A. Mandoli, A. H. M. de Vries, R. Naasz, B. Feringa, *Tetrahedron* **2000**, *56*, 2865–2878.

[11] C. Claver, E. Fernandez, A. Gillon, K. Heslop, D. J. Hyett, A. Martorell, A. G. Orpen, P. G. Pringle, *Chem. Commun.* **2000**, 961–962.

[12] a) B. Hagemann, K. Junge, S. Enthaler, M. Michalik, T. Riermeier, A. Monsees, M. Beller, *Adv. Synth. Catal.* **2005**, *347*, 1978–1986; b) K. Junge, G. Oehme, A. Monsees, T. Riermeier, U. Dingerdissen, M. Beller, *Tetrahedron Lett.* **2002**, *43*, 4977–4980; c) K. Junge, G. Oehme, A. Monsees, T. Riermeier, U. Dingerdissen, M. Beller, *J. Organomet. Chem.* **2003**, *675*, 91–96; d) K. Junge, B. Hagemann, S. Enthaler, G. Oehme, M. Michalik, A. Monsees, T. Riermeier, U. Dingerdissen, M. Beller, *Angew. Chem.* **2004**, *116*, 5176–5179; *Angew. Chem. Int. Ed.* **2004**, *43*, 5066–5069; e) B. Hagemann, K. Junge, S. Enthaler, M. Michalik, T. Riermeier, A. Monsees, M. Beller, *Adv. Synth. Catal.* **2005**, *347*, 1978–1986; f) S. Enthaler, G. Erre, K. Junge, D. Michalik, A. Spannenberg, F. Marras, S. Gladiali, M. Beller, *Tetrahedron: Asymmetry* **2007**, *18*, 1288–1298; g) S. Enthaler, G. Erre, K. Junge, J. Holz, A. Börner, E. Alberico, I. Nieddu, S. Gladiali, M. Beller, *Org. Process Res. Dev.* **2007**, *11*, 568–577.

[13] A. Wolfson, I. F. J. Vankelecom, S. Geresh, P. A. Jacobs, *J. Mol. Catal. A* **2003**, *198*, 39–45.

[14] A. Wolfson, I. F. J. Vankelecom, S. Geresh, P. A. Jacobs, *J. Mol. Catal. A* **2004**, *217*, 21–26.

[15] L. Bartek, M. Drobek, M. Kuzam, P. Kluson, L. Cerveny, *Catal. Commun.* **2005**, *6*, 61–65.

[16] M. T. Ashby, J. Halpern, *J. Am. Chem. Soc.* **1991**, *113*, 589–594.

[17] X. Dong, C. Erkey, *J. Mol. Catal. A* **2004**, *211*, 73–81.

[18] F. H. Mahfud, F. Ghijsen, H. J. Heeres, *J. Mol. Catal. A* **2007**, *264*, 227–236.

[19] http://cea.grc.nasa.gov/index.html, accessed 4.5.08.

[20] G. Combes, E. Coen, F. Dehghani, N. Foster, *Ind. Eng. Chem. Res.* **2006**, *45*, 1281–1290.